Supplement of Atmos. Meas. Tech., 10, 1359–1371, 2017
http://www.atmos-meas-tech.net/10/1359/2017/
doi:10.5194/amt-10-1359-2017-supplement


Atmospheric Measurement Techniques
Open Access

*Supplement of*

# Analysis of geostationary satellite-derived cloud parameters associated with environments with high ice water content

**Adrianus de Laat et al.**

*Correspondence to:* Adrianus de Laat (laatdej@knmi.nl)

## Supplementary Information.

### S1.1 Analysis of AIRBUS in-service events

AIRBUS provided a database of 59 reported events of in-service icing. Because of confidentiality issues, the database is not public. However, in case of interest, AIRBUS can be contacted about details of the database or the events (Alice Calmels, AIRBUS)

As a first step, the cases from the AIRBUS event database were evaluated, which in total covers 59 events. Of those events, about half fell outside the SEVIRI disc (29 of 59). Of the remaining 30 events, two were suspect, and for 19 events no daytime measurements were available, leaving nine (9) events for which MSG-CPP data was available.

A detailed meteorological and data analysis of all 30 events within the SEVIRI disc was then performed. The database contains a brief meteorological analysis of the event, images of all available MSG measurements surrounding the event (± 3 hours) for a ± 2° area around the event location of brightness temperatures and MSG-CPP parameters (if available). These images serve to identify and characterize the type of convection and convective activity of the event. Furthermore, time series of spatial average brightness temperatures and average MSG-CPP parameters (if available) were provided for ± 3 hours around the event, and averages were calculated for measurements within a radius of 10 km, 25 km, 50 km and 100 km. The purpose for the time series is to identify the stage of the convective activity (developing, mature, aging).

Figure S1a shows an example of the MSG-CPP measurements of event 31. This event clearly occurred right over a deep and strong convective event, with widespread iced cloud tops, high CWP values, high COT, high clouds, cold cloud tops and strong precipitation.

Figure S1b shows the time series of area average MSG-CPP parameters. Most parameters are fairly constant over the time period and independent of the area of averaging, indicative of mature large scale convection. When looking near the location of this event (radius < 10 km), we do see that both the COT and CWP were increasing near the event, indicating that the convection was still active.

The nine events for which MSG-CPP data was available were further evaluated in detail to determine similarities between these nine events. Figure S2 shows a scatter plot of various MSG-CPP parameters falling within a 100 km radius of the event location. Panel (A) shows that the closer the measurements to the event, the higher the CWP. Typically MSG-CPP CWP is larger than 1000 $g/m^2$ near the events. Panel (B) shows that in general these clouds are cold clouds, with cloud top temperatures below -40°C (233 K), and cloud heights of 8 km or higher. Panel (C) shows that precipitation is directly related to the CWP, as expected [Roebeling et al., 2006; Meirink, 2013]. Precipitation thus is not an independent parameter in the MSG-CPP measurements. Finally, for all cases there the effective radius is > 10 μm.

**S1.2 Construction of a provisional High IWC mask**

Based on the analysis presented in the previous section, a first MSG-CPP High IWC mask was constructed. An MSG-CPP pixel is identified as potentially containing high IWC under the five conditions listed in table S2.

Figure S3 shows an example of how these criteria subsequently decrease the number of MSG-CPP measurements identified as high IWC events for AIRBUS event 31. Figure S4 shows the last panel of Figure 3 but then for the entire SEVIRI disc. Clearly the High IWC mask strongly reduces the number high IWC events. The strongest reductions in pixels are related to the requirement of cloud phase being ice, the cloud water path > 1000 g/m$^2$ and the cloud top height > 8 km and cloud top temperature < 225. Note that the cloud top height and cloud top temperature are locally interchangeable.

Finally, Figure S5 shows the High IWC mask as in Figures S3 and S4 for all nine AIRBUS events for which MSG-CPP is available. Unsurprisingly, all nine cases occur in areas identified by the High IWC mask.

Although the High IWC mask as defined here identifies potential high IWC events in a way that appears consistent with expectations, the limited number of AIRBUS events on which the High IWC mask is based means that there is room for further refinement, for which an alternative approach is needed as there are currently no other events available for analysis. Within the HAIC consortium it was decided that the 'next best thing' was to compare and evaluate the High IWC mask with radar and lidar observations from polar orbiting satellites.

**S1.3 Evaluation of MSG-CPP with DARDAR**

Although it is not the primary objective of this paper to verify CPP with DARDAR data, we nevertheless provide some comparisons to get a sense of how these two products relate to each other.

DARDAR combines vertical information from the CLOUDSAT radar and CALIPSO lidar measurements into one product. Both instruments are part of the Polar orbiting A-train constellation. A test dataset was constructed, consisting of 31 daytime orbits in the year 2008, covering all months, randomly distributed throughout the SEVIRI disc, and containing a sufficient number of high IWC measurements within one orbit (see supplementary information table S2).

Figure S6 shows an example of a DARDAR orbit and the corresponding MSG-CPP cloud top heights. Indicated are also the locations where the DARDAR profiles indicate ice clouds. Based on visual inspection there is a clear correspondence between the DARDAR ice identification and the MSG-CPP clouds. Note that because of the time it takes for one DARDAR orbit to circle the earth, and with a MSG-SEVIRI acquisition every 15 minutes, typically three to five MSG-CPP images cover the DARDAR orbit, which means that for some DARDAR profiles the MSG-CPP image shown in Figure S6 is not the MSG-CPP output data nearest in time to the DARDAR measurement.

Figure S7 shows the same DARDAR orbit but now with the vertical ice water content profile and the corresponding MSG-CPP cloud top height (CTH). Also here there is a clear correspondence between mid-latitude DARDAR maximum ice cloud heights and MSG-CPP cloud top heights. However, within the tropics MSG-CPP frequently underestimates the maximum ice cloud height as observed with DARDAR. This typically occurs for less dense cirrus and is related to the very nature of the MSG-CPP cloud top temperature/height algorithm. The CPP cloud height algorithm is a simple one-channel (10.8 micron) approach, which assumes opaque clouds. Top-of-atmosphere IR radiation for semi-transparent cirrus contains a significant contribution from the warm surface, leading to an overestimation of the cloud top temperature and underestimation of the cloud height. Such an underestimation of cloud top height and overestimation of cloud top temperature is typical for the many SEVIRI-based cloud properties algorithms, as evaluated in Hamann et al. [2014].

Figure S8 shows the probability distribution of DARDAR cloud top height (maximum level with IWC > 0) and MSG-CPP cloud top height as function of the MSG-CPP High IWC mask parameter threshold values. The parameters with the largest impact on the probability distribution are the CWP and the cloud top height and/or cloud top temperature, as was already noted before. Obviously the detection is sensitive to choice of height/temperature threshold in this comparison. To provide some background: low clouds and high (optically) thick cirrus clouds typically have a condensed water path of at maximum few hundred $g/m^2$. Optically thin cirrus clouds have typically a CWP of less than 100 $g/m^2$. Only for very deep and thick convective clouds the CWP exceeds 1000 $g/m^2$. When looking at specific CWP values, we see that a given threshold improves the comparison but that it is unclear which of the thresholds is better as the correlation between DARDAR and MSG-CPP cloud top heights hardly differ for different CWP thresholds (not shown).

To further investigate the CWP in both MSG-CPP and DARDAR, the DARDAR IWC profiles were converted to total IWP and then compared to the MSG-CPP CWP. Figure S9 shows the probability distribution of MSG-CPP and DARDAR IWP for the same data used for Figure S8. The probability distribution is clearly skewed, with DARDAR IWP being considerably larger than the MSG-CPP CWP. One possible explanation is that for its retrieval, the MSG-CPP algorithm assumes a vertically homogeneous distribution of effective radius and cloud condensate, which may be unrealistic. Because there is less reflected sunlight (information) coming from deeper in the clouds towards the satellite [Platnick, 2000], the satellite measurements will be more representative of the upper part of in particular deep convective clouds. However, the size of ice particles within geometrically thick clouds will generally be larger towards the cloud bottom [Feofilov et al., 2015] due to various processes (*e.g.*

sedimentation and the higher water vapor pressure at lower altitudes). Hence, the MSG-CPP algorithm likely underestimates the average effective radius of these optically thick clouds. The parameterization of the MSG-CPP CWP depends linearly on the retrieved effective radius, possibly explaining the MSG-CPP underestimation of CWP.

To test this idea we further analyzed Figure S9 for its relation with the variability in the effective radius of the DARDAR profile. The root-mean-square (rms) value of the effective radius of the profile for where there is ice provides an indication of how uniform the effective radius distribution is throughout the profile. In Figure S10 the probability distribution of Figure S9 is filtered on the rms value of the DARDAR profile effective radius: the smaller the rms value, the more uniform the vertical distribution of the effective radius is and the more it can be expected that the DARDAR CWP/IWP agrees with MSG-CPP. Figure 5 shows that this indeed is the case. Furthermore, it appears that the vertical effective radius variability acts approximately as an offset: the fit lines through the data are more or less parallel to the 1:1 line.

The analysis performed in this section provides a brief characterization of the MSG-CPP data vs. DARDAR measurements, highlighting agreement as well as caveats. With this information, the next step is to investigate to what extent the first High IWC mask is capable of identifying high IWC values in the DARDAR IWC profiles, and whether the mask can be improved.

| CPP variable | Threshold value |
| --- | --- |
| Cloud Phase | ice |
| Effective Radius | > 10 μm |
| Condensed Water Path | > 1000 $g/m^2$ |
| Cloud Top Height | > 8 km |
| Cloud Top Temperature | < 225 K |

**Table S1:** CPP threshold values for the High IWC mask v1.

| YEAR | MONTH | DAY | HH:MM:SS |
|---|---|---|---|
| 2008 | 01 | 02 | 09:18:01 |
| 2008 | 01 | 02 | 12:35:48 |
| 2008 | 01 | 03 | 13:19:04 |
| 2008 | 01 | 03 | 14:57:57 |
| 2008 | 01 | 03 | 16:36:50 |
| 2008 | 01 | 04 | 12:23:27 |
| 2008 | 01 | 05 | 16:24:30 |
| 2008 | 02 | 02 | 13:31:39 |
| 2008 | 02 | 02 | 16:49:25 |
| 2008 | 02 | 04 | 11:40:25 |
| 2008 | 02 | 05 | 10:44:47 |
| 2008 | 02 | 05 | 15:41:26 |
| 2008 | 03 | 02 | 13:00:45 |
| 2008 | 03 | 02 | 16:18:31 |
| 2008 | 04 | 01 | 09:55:30 |
| 2008 | 04 | 03 | 14:39:50 |
| 2008 | 04 | 03 | 16:18:43 |
| 2008 | 05 | 01 | 11:47:09 |
| 2008 | 05 | 02 | 14:09:18 |
| 2008 | 05 | 03 | 16:31:27 |
| 2008 | 05 | 04 | 13:56:57 |
| 2008 | 06 | 11 | 16:37:42 |
| 2008 | 09 | 02 | 15:31:07 |
| 2008 | 09 | 02 | 17:10:00 |
| 2008 | 10 | 04 | 10:34:40 |
| 2008 | 10 | 04 | 15:31:19 |
| 2008 | 10 | 04 | 17:10:12 |
| 2008 | 11 | 02 | 11:43:07 |
| 2008 | 12 | 01 | 11:12:50 |
| 2008 | 12 | 01 | 14:30:37 |
| 2008 | 12 | 03 | 12:39:24 |

**Table S2**. Dates of equator crossing time of DARDAR orbits used for detection of High IWC events in MSG-CPP.

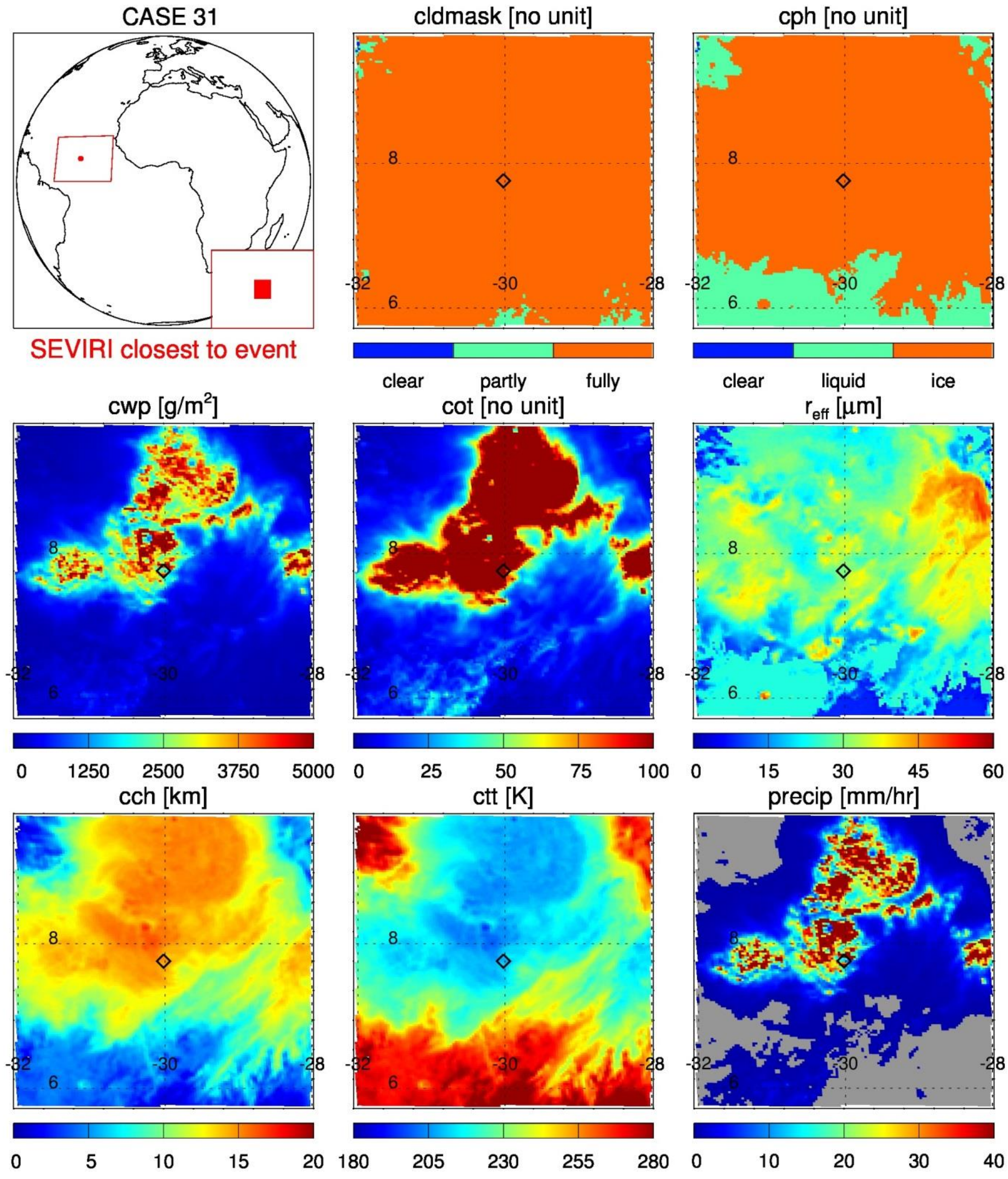


**Figure S1a. Nearest** MSG-CPP measurements for AIRBUS event 31. CWP = Cloud Water Path, COT = Cloud Optical Thickness, $r_{eff}$ = effective radius, CCH = Cloud Column Height, CTT = Clout Top Temperature, precip = precipiation.

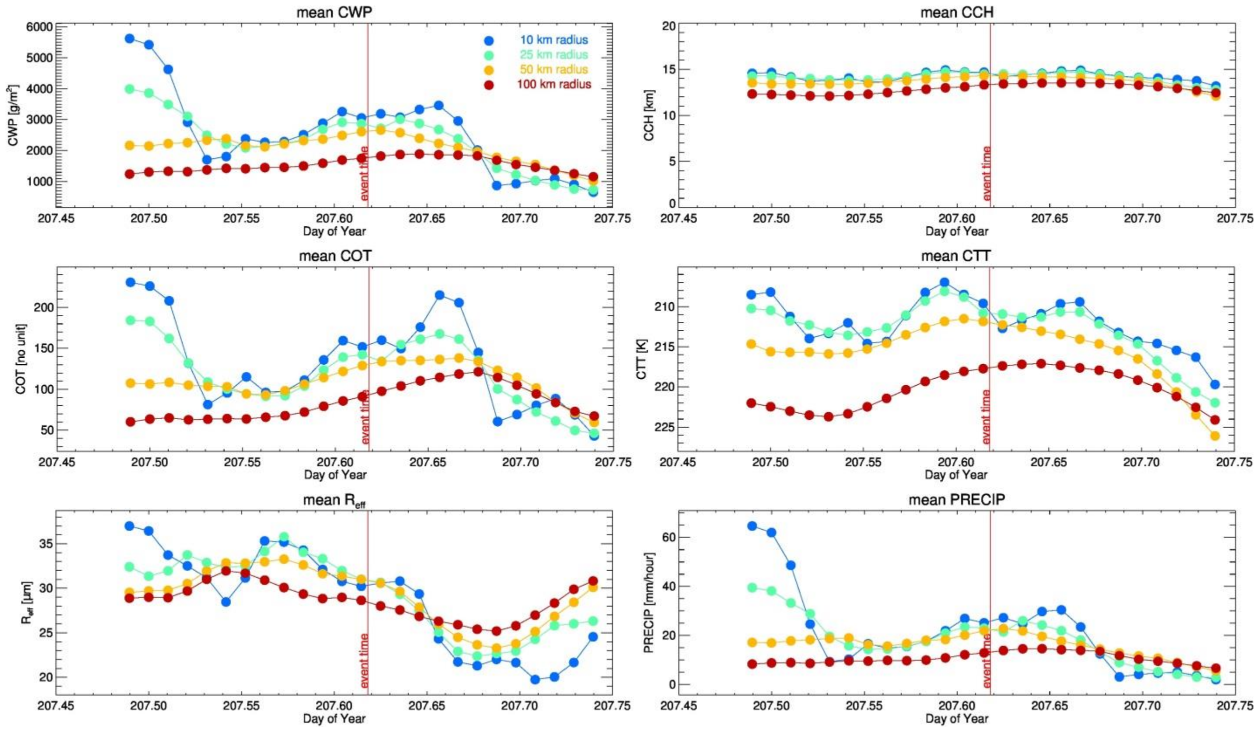


**Figure S1b**. Time series of area average MSG-CPP parameters for AIRBUS event 31 for the period ± 3 hours around the event and the areas with radii of < 10 km, < 25 km, < 50 km and < 100 km.

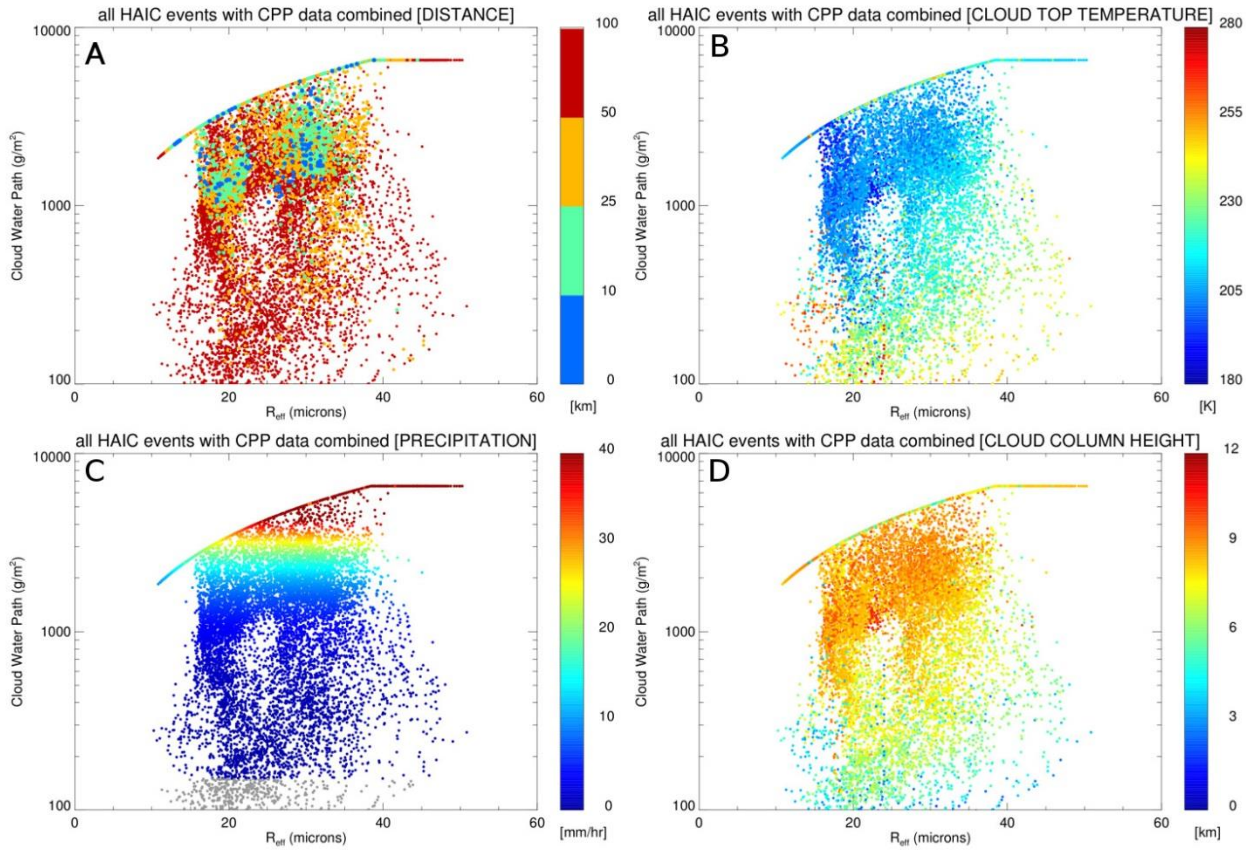


**Figure S2**. Scatterplots of MSG-CPP parameters for the nine AIRBUS events for which MSG-CPP data is available. Only the MSG-CPP measurements closest to the event were taken. All panels show the CWP ($g/m^2$) as function of the effective radius (μm). The color coding indicates a third parameters: (A) radius within which MSG-CPP measurements were taken (km; distance to event location), (B) cloud top temperature (K), (C) precipitation (mm/hr) and (D) cloud column height (km). The upper line denotes a theoretical limit to the MSG-CPP relation between CWP and the effective radius.

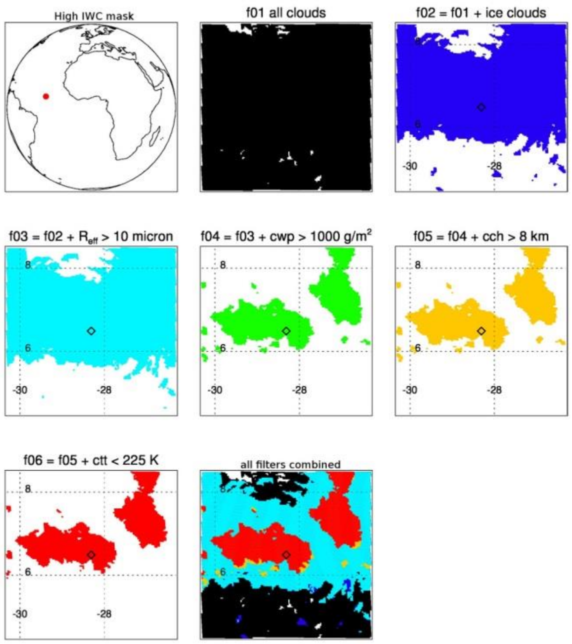


**Figure S3.** Filters applied for the of High IWC mask for AIRBUS event 31. Each panel indicates the filter applied as in the title compared to the previous panel. The first panel shows the region of interest, the last panel shows how each pixel is characterized.

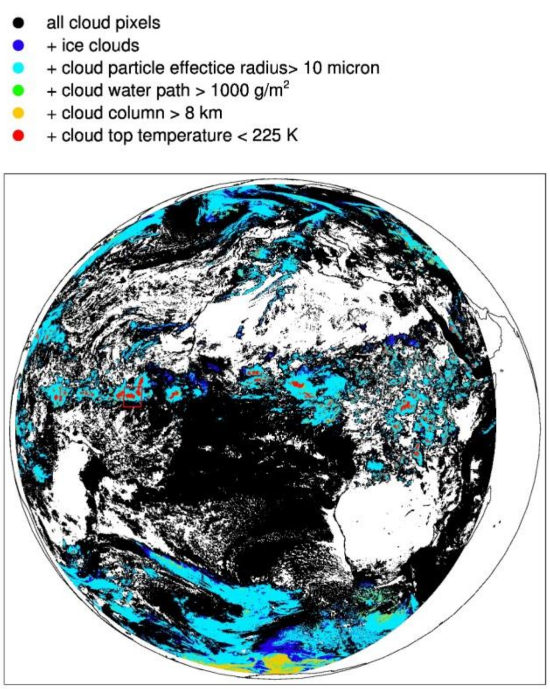

**Figure S4.** As the last panel of Figure S3 but for the entire SEVIRI disc.

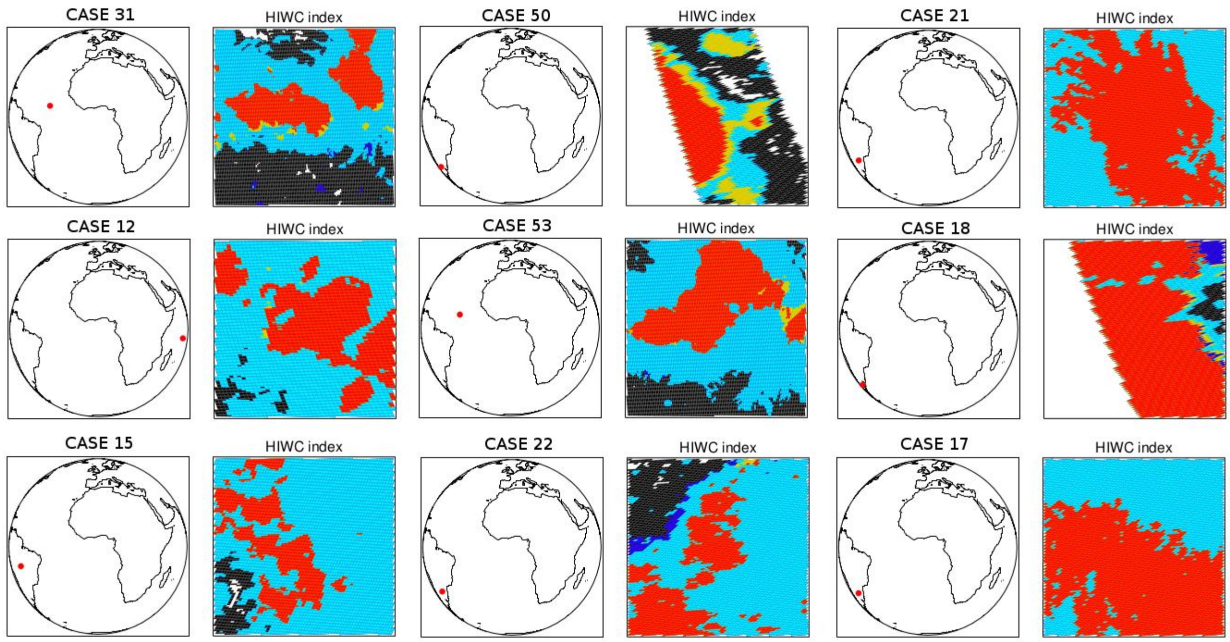


**Figure S5.** As Figure S3, first and last panels, but for all nine AIRBUS events for which MSG-CPP data is available (see table S2). Color coding as in Figures S3 and S4.

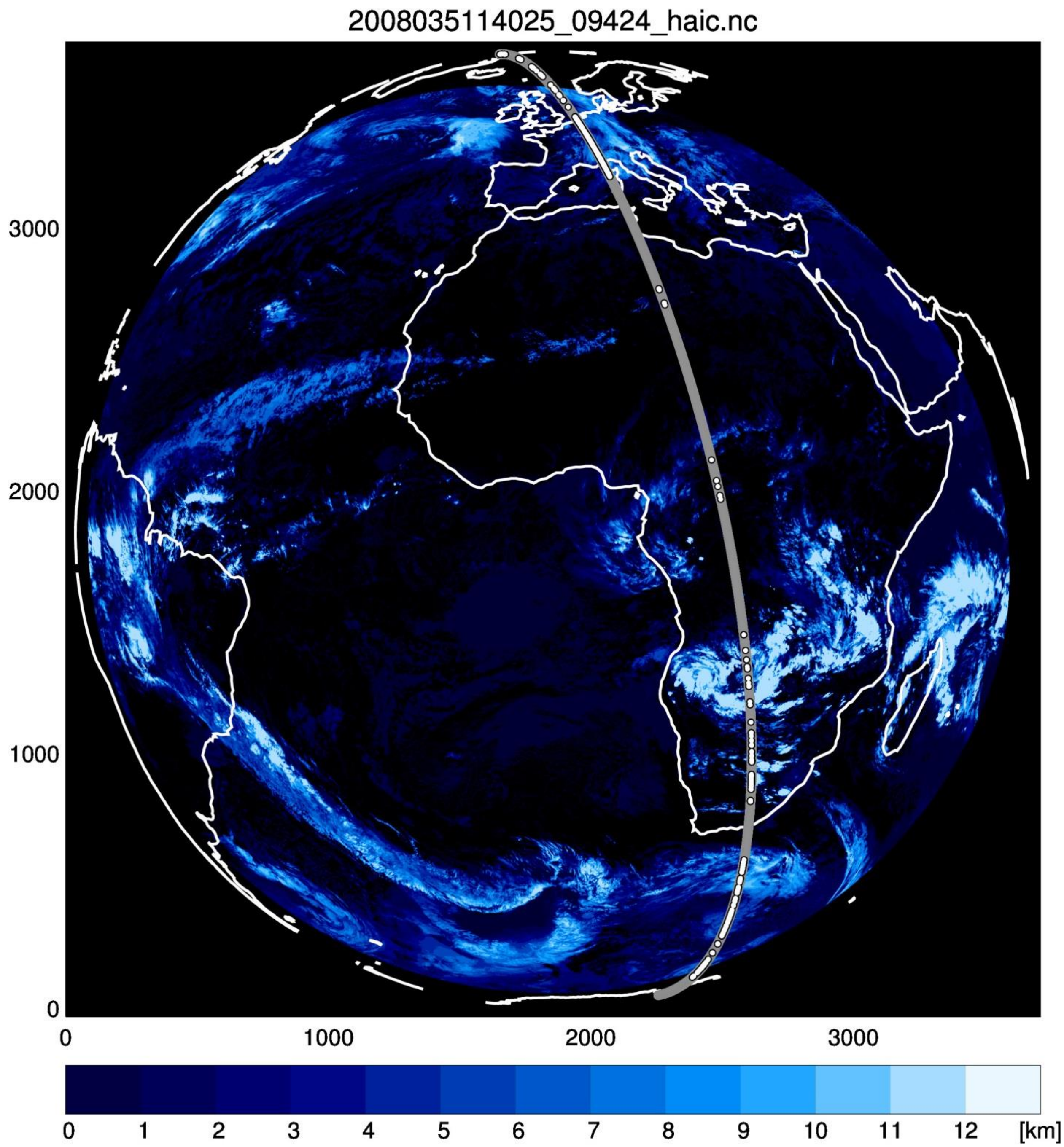


**Figure S6.** DARDAR orbit (4 February 2008, 12:29:56 UTC equator crossing time) and corresponding MSG-CPP cloud top height (4 February 2008, 12:30 UTC). The DARDAR orbit is shown by the grey line, with black-white dots indicating DARDAR profiles with ice in it. Note that the time of MSG-CPP image is nearest to the DARDAR equator crossing time.

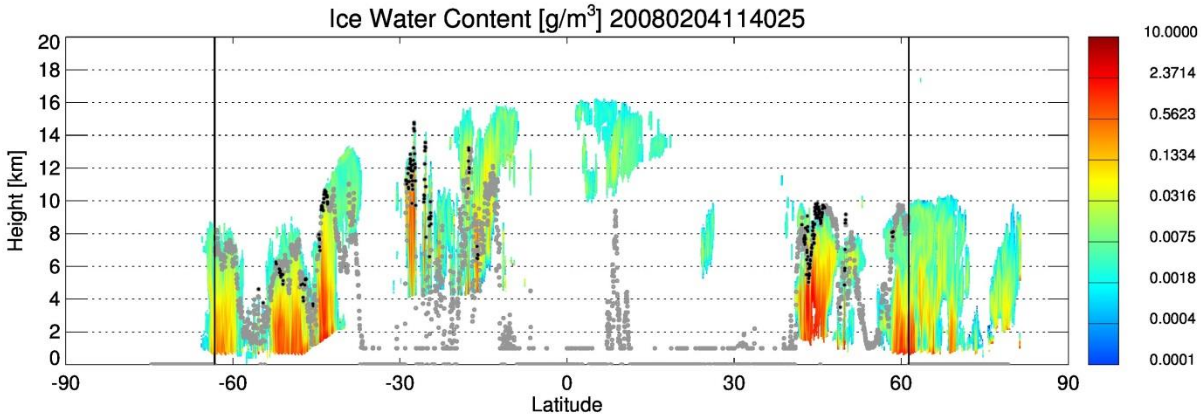


**Figure S7.** Cross section of DARDAR ice water content and corresponding MSG-CPP cloud top height (grey/black dots) as shown in Figure S6. The black dots denote the MSG-CPP pixels for which the High IWC mask was identified. The vertical bars indicate the geographical range for which MSG-CPP measurements are available due to the need of MSG-CPP for daytime observations.

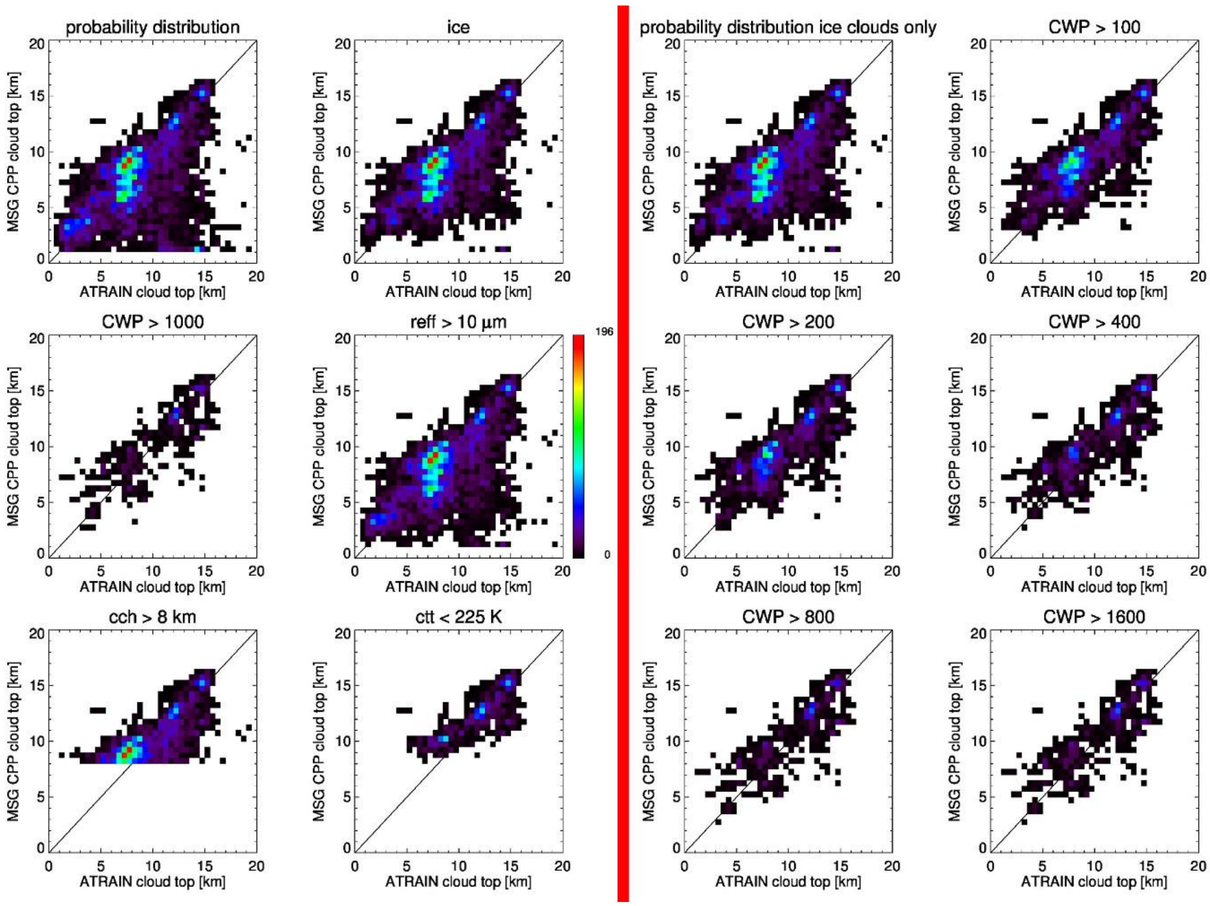


**Figure S8.** Probability distribution of cloud top heights estimated from MSG-CPP and A-Train/DARDAR data (highest level with IWC > 0) as function of MSG-CPP parameter values for approximately 160,000 DARDAR profile measurements obtained from 31 DARDAR orbits. The left section shows the effect of the different High IWC mask thresholds, the right section shows the effect of different CWP thresholds.

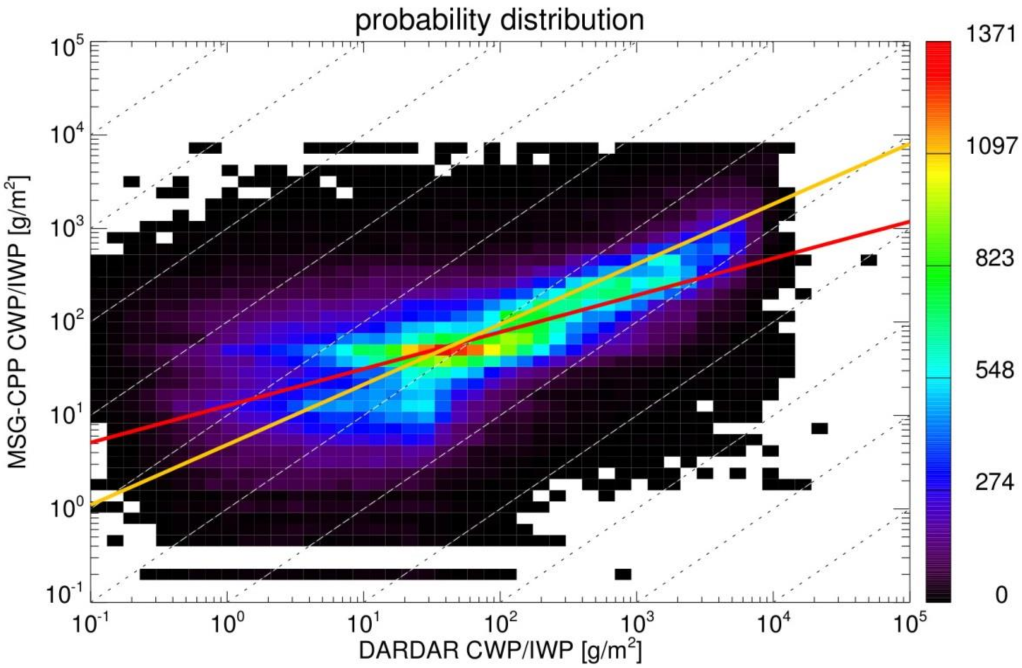


**Figure S9.** Probability distribution of CWP or IWP from MSG-CPP vs DARDAR for the orbits in table 1 combined. Two different linear fits are indicated with (orange) and without (red) forcing intercept of zero, but are for visualization purposes only.

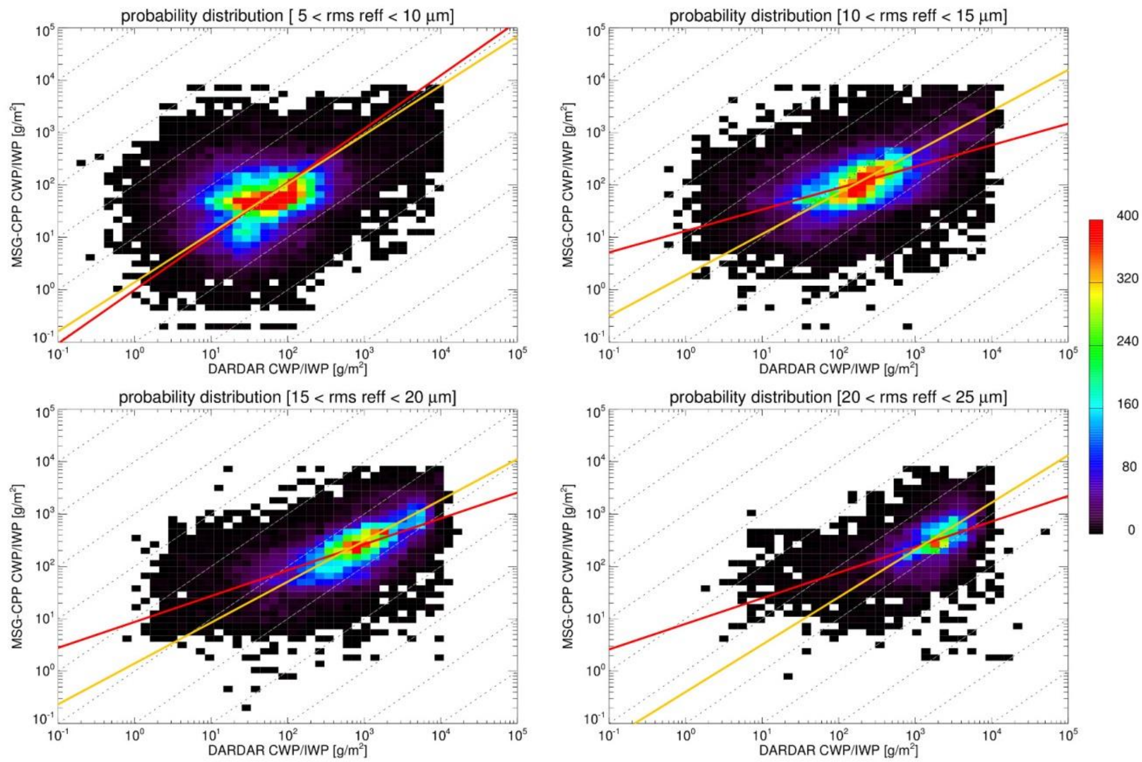


**Figure S10.** As Figure S9 but filtered according to the root-mean-square value of the effective radius of each DARDAR effective radius profile.